https://doi.org/10.22226/2410-3535-2022-4-367-372

Optical and electrical properties of a new complex oxide $Pb_{1/3}Na_{1/3}K_{1/3}Ta_{2/3}Fe_{1/3}O_{3-\delta}$ with perovskite structure

N. A. Zhuk[†,1], A. M. Popov[1], R. I. Korolev[1], V. V. Moroz[1], A. A. Selyutin[2], A. V. Koroleva[2], N. A. Sekushin[3], B. A. Makeev[4]

[†]nzhuck@mail.ru

[1]Syktyvkar State University, Syktyvkar, 167001, Russia
[2]Saint Petersburg State University, St. Petersburg, 199034, Russia
[3]Institute of Chemistry of the Komi Science Center UB RAS, Syktyvkar, 167982, Russia
[4]Institute of Geology of the Komi Science Center UB RAS, Syktyvkar, 167982, Russia

A cubic perovskite of complex composition $Pb_{1/3}Na_{1/3}K_{1/3}Ta_{2/3}Fe_{1/3}O_{3-\delta}$ (sp. gr. *Pm*-3*m*, *a* = 3.9767(3) Å) was synthesized for the first time by the solid-phase reaction method. The samples are characterized by an almost pore-free microstructure formed by slightly melted randomly oriented cubic crystallites. The band gap (≈2.05 eV) of a complex perovskite for a direct allowed electronic transition was calculated from the data of the diffuse reflection spectrum. According to impedance spectroscopy data, three polarization processes are observed in the sample at room temperature: low-frequency (at a frequency less than 300 Hz), medium-frequency (from 300 Hz to 10 kHz), and high-frequency (from 100 kHz to 10 MHz) ones. The permittivity of the sample at room temperature and a frequency of 10^7 Hz reaches high values of about 147, and the dielectric loss tangent does not exceed 0.12.

Keywords: perovskite, iron, lead, dielectric properties, optical properties, diffuse reflection spectrum.

1. Introduction

Materials with low dielectric loss, high dielectric constant and low temperature coefficient of resonant frequency are increasingly required for the use as dielectric resonators. Using a compact and highly efficient resonator composed of these materials, reliable microwave devices can be easily fabricated [1–4]. These requirements are best met by compounds with the perovskite structure [1–3, 5, 6]. For example, the $Ba(Zn_{1/3}Ta_{2/3})O_3$ ceramic has excellent microwave dielectric properties for microwave applications exhibiting a dielectric constant of 30, a temperature coefficient of resonant frequency of 0–0.5 ppm/°C, and a quality factor of $Q \approx 6500$ [1]. The perovskite structure is suitable for the formation of ferroelectric properties. In lead-containing perovskites, such as $PbTiO_3$, $PbZrO_3$, $BaNbO_3$ and a number of isomorphic solid solutions such as $(Ba, Pb)TiO_3$ or $Ba(Ti, Zn)O_3$, the maximum values of practically useful pyroelectric, piezoelectric, and dielectric parameters are achieved. A significant disadvantage of such ceramics is the lead content [4].

Traditionally, perovskites are described by the general formula ABO_3 (sp.gr. *Pm*-3*m*), in which A is a large electropositive cation (A — Pb, Ba, Sr) and B is a small transition metal ion (B — Nb, Ta, Zr) [7–14]. In the crystal structure of perovskite, there is a framework of BO_6 octahedra connected by axial vertices, in the cuboctahedral voids of which large A cations are located. The tolerance of the perovskite crystal structure to various kinds of isomorphic substitutions both in A and B cationic sublattices, high tolerance to defects, makes it possible to form many combinations of compositions with various physicochemical properties, opening up prospects and possibilities for the chemical design of materials based on perovskites. In this regard, mixed perovskites $AB'_{1/2}B''_{1/2}O_3$ and $AB'_{1/3}B''_{2/3}O_3$ are known, in which 1/2 or 1/3 of the octahedral positions B are occupied by cations with similar polarization properties (B' — Mg, Ln, 3d ions) [15–20]. In particular, perovskites of the composition $A(Fe_{1/2}Ta_{1/2})O_3$ (A — Ba, Sr, and Ca) are known, which exhibit microwave dielectric properties [21–25]. This article shows for the first time the possibility of synthesizing the complex perovskite $Pb_{1/3}Na_{1/3}K_{1/3}Ta_{2/3}Fe_{1/3}O_3$ by the ceramic method, in which positions B are occupied by Ta (V) and Fe (III) ions in a ratio of 2:1, and in ions Pb (II), Na (I) and K (I) are distributed in positions A in equal proportions, and the results of a study of its optical and dielectric properties at room temperature.

2. Materials and methods

The complex oxide $Pb_{1/3}Na_{1/3}K_{1/3}Ta_{2/3}Fe_{1/3}O_{3-\delta}$ with the perovskite structure was synthesized by the standard solid-state reaction or route, from oxides of iron (III), tantalum (V), and lead (II) nitrate, potassium and sodium carbonate and bicarbonate. Precursors were thoroughly homogenized in a jasper mortar for one hour. The mixture obtained was pressed into disks and calcined in air in crucibles. The

heat treatment of the samples was carried out in several stages at 650, 950, and 1050°C, respectively. At each stage of calcination, the samples were again finely ground and compacted. X-ray phase analysis was carried out using a Shimadzu 6000 X-ray diffractometer (Cu K_α radiation; $2\theta = 10 - 70°$; scanning speed 2.0°/min). The unit cell parameters of perovskite were calculated using the CSD software package [26]. XPS analysis was performed using a Thermo Scientific ESCALAB 250Xi X-ray spectrometer (Escalab 250Xi, Thermo Fisher Scientific, United Kingdom, Avantage v5.9925) (Al K_α radiation, 1486.6 eV). An ion-electronic charge compensation system was used to neutralize the charge of the sample. All peaks in the spectrum are calibrated relative to the C 1s peak at 284.6 eV. The ESCALAB 250 Xi software was used to process the experimental data. Surface morphology studies of preparations and local quantitative elemental analysis were carried out by scanning electron microscopy and energy dispersive X-ray spectroscopy (scanning electron microscope Tescan VEGA 3LMN, energy dispersive spectrometer INCA Energy 450). To study the electrical properties, a conductive silver layer is deposited on both sides of the ceramic disk by firing silver paste at 600°C for an hour. The measurements were carried out using an E7–28 impedance meter (frequency range $25 - 10^7$ Hz) at a temperature of 25°C. Diffuse reflectance spectra were recorded in the range of 200 – 900 nm using a Shimadzu UV-2550 spectrophotometer with a spectral step of 1 nm. Halogen and deuterium lamps were used as the radiation source. The spectra were obtained for substances in a barium sulfate matrix. The scattering spectrum from the pure barium sulfate matrix was subtracted from the resulting spectrum. For a quantitative description of the diffuse scattering spectra, the basis of the Kubelka-Munk theory was applied. The value of E_g was determined by the position of the fundamental absorption edge according to the Tauc equation $(h\nu F(r))1/n = A(h\nu - E_g)$, where E_g is the band gap, h is Planck's constant, ν is the oscillation frequency of electromagnetic waves, $F(r) = (1-r)^2/2r$ is the Kubelka-Munk function, A is a constant. The exponent value for direct allowed transitions is $n = 1/2$. The diffuse scattering spectra were rearranged in Tauc coordinates: $(h\nu F(r))^2$ versus E (eV). The E_g value was determined by extrapolating the linear section of the Tauc curve to the energy axis.

3. Results and discussion

As X-ray phase analysis showed, the $Pb_{1/3}Na_{1/3}K_{1/3}Ta_{2/3}Fe_{1/3}O_{3-\delta}$ sample was crystallized in the structural type of cubic perovskite (sp. gr. *Pm*-3*m*), no reflections of impurity phases were found. The X-ray pattern of the sample is shown in Fig. 1.

The unit cell parameter of the synthesized perovskite was 3.9767 ± 0.0003 Å, which is close to the unit cell parameters of known perovskites $KTaO_3$ ($a = 3.989$ Å), $SrFe_{0.5}Ta_{0.5}O_3$ ($a = 3.9730$ Å) [2]. Apparently, large Na (I), K (I), Pb (II) ions occupy cuboctahedral A positions in the perovskite structure ($R(K(I)_{c.n.-12} = 0.164$ nm, $Na(I)_{c.n.-12} = 0.139$ nm, $Pb(II)_{c.n.-12} = 0.149$ nm), while Fe (III), Ta (V) ions occupy octahedral B positions in the perovskite block ($R(Ta(V)_{c.n.-6} = 0.064$ nm, $R(Fe(III)_{c.n.-6} = 0.0645$ nm) [27]. The preferential placement of iron (III) ions in octahedral sites was previously confirmed by the example of complex oxides of various crystal structures [28 – 31]. The charge state of Fe (III) ions in perovskite was confirmed by the XPS method (Fig. 2). An analysis of the spectra of the complex

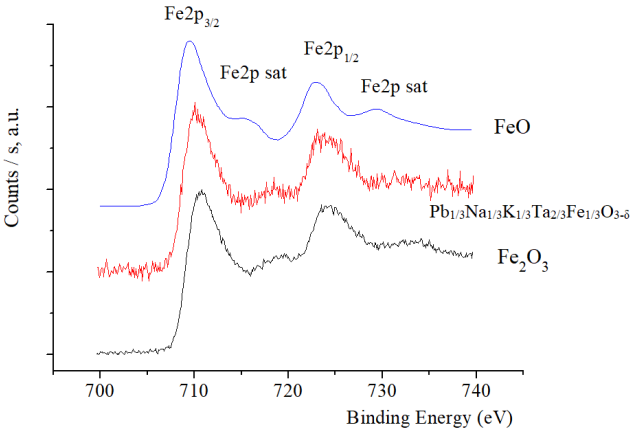

Fig. 2. (Color online) Fe2p spectra of $Pb_{1/3}Na_{1/3}K_{1/3}Ta_{2/3}Fe_{1/3}O_{3-\delta}$ sample.

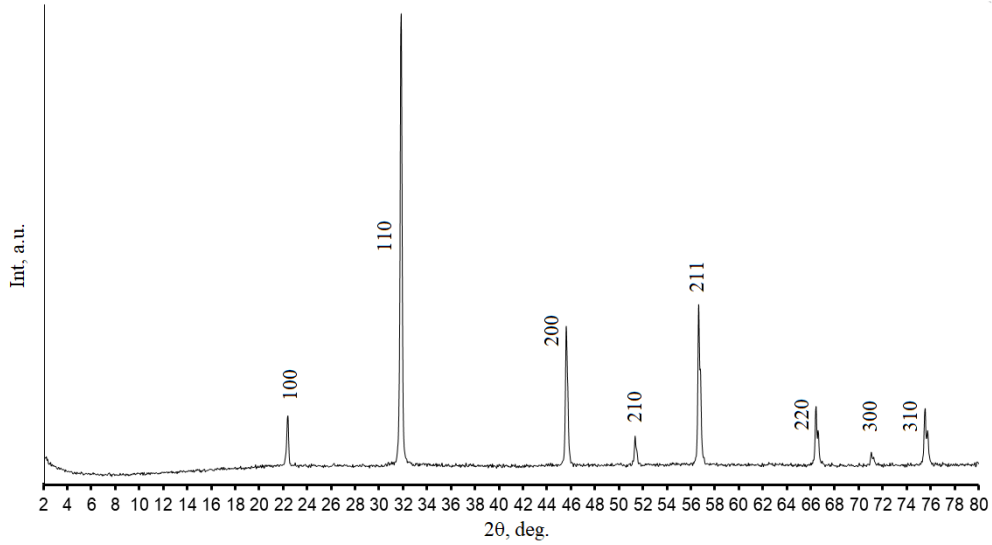

Fig. 1. X-ray diffraction pattern for the $Pb_{1/3}Na_{1/3}K_{1/3}Ta_{2/3}Fe_{1/3}O_{3-\delta}$ sample.

oxide with the spectra of oxides Fe_2O_3 and FeO [32] showed that the spectrum of perovskite is in good agreement both in the number and energy position of the main features with the spectrum of iron (III) oxide Fe_2O_3, which suggests that the iron atoms are in the same charge state with an effective charge of +3. In particular, the Fe_2O_3 oxide and perovskite have the same absorption lines at 711 and 725 eV. Perovskite does not exhibit satellite lines at 716 and 730 eV, which are characteristic of divalent Fe^{2+} ions [33].

As studies by scanning electron microscopy showed, the microstructure of the sample was practically non-porous and was formed by slightly melted cubic crystallites (Fig. 3). Despite this grain shape, due to heterogeneity in size, they are quite densely packed. The size of individual grains reaches from 1 to 5 μm. Mapping over the surface of the sample showed a uniform distribution of the elements that make up the ceramics (Fig. 4).

The sample was practically pore-free, the porosity of $Pb_{1/3}Na_{1/3}K_{1/3}Ta_{2/3}Fe_{1/3}O_{3-\delta}$, according to SEM, was equal to ≈7 percent (Fig. 5).

The diffuse reflectance spectra of the $Pb_{1/3}Na_{1/3}K_{1/3}Ta_{2/3}Fe_{1/3}O_{3-\delta}$ sample are shown in Fig. 6.

The band gap (≈2.05 eV) of iron-containing perovskite for a direct allowed electronic transition was estimated from the data of the diffuse reflection spectrum (Fig. 6). As the figure shows, the sample is characterized by significant reflection in the areas of yellow (565 – 590 nm) and red (635 – 770 nm) colors. Apparently, the reflection in the yellow and long-wavelength visible range is associated with the yellow-brown color of the sample. The sample has a complex absorption peak with a barely distinguishable shoulder at 650 nm and a maximum at 450 nm, related to the d-d transition $^6A_{1g} \rightarrow {}^4T_{2g}$, which indicates the presence of iron ions in the trivalent state (Fe^{3+}) with octahedral symmetry [34]. The underestimated

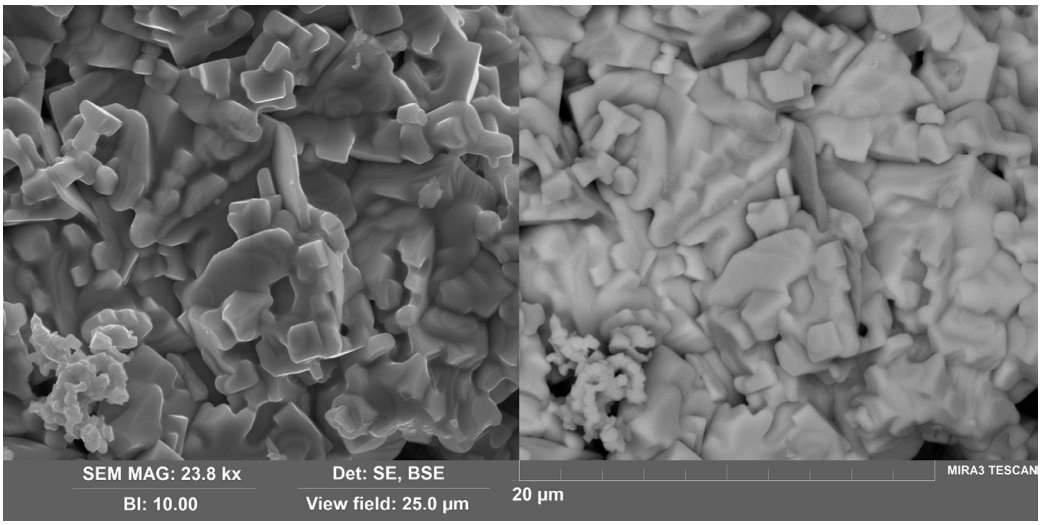

Fig. 3. Micrographs of the surface of a $Pb_{1/3}Na_{1/3}K_{1/3}Ta_{2/3}Fe_{1/3}O_{3-\delta}$ sample in the mode of secondary and elastically reflected electrons.

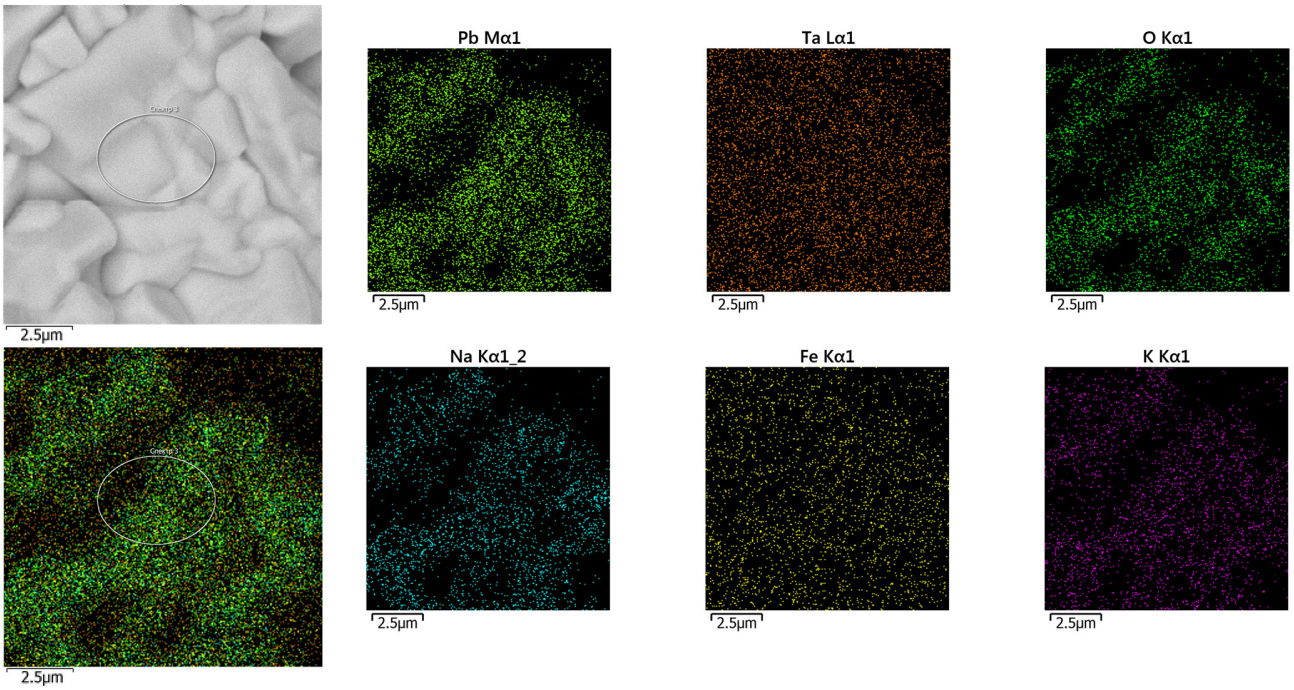

Fig. 4. (Color online) Sample elemental mapping results of $Pb_{1/3}Na_{1/3}K_{1/3}Ta_{2/3}Fe_{1/3}O_{3-\delta}$.

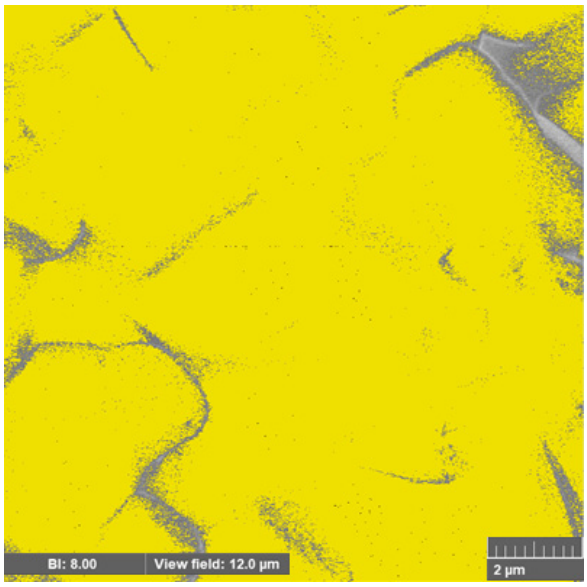

Fig. 5. (Color online) Porosity of the $Pb_{1/3}Na_{1/3}K_{1/3}Ta_{2/3}Fe_{1/3}O_{3-\delta}$ sample according to SEM data (gray areas).

values of the band gap in the investigated perovskites can be a consequence of the Stark effect, as well as the small grain sizes of ceramics. The band gap of the studied ceramics correlates with the energy of solar radiation, which has a maximum intensity (2.1–2.5 eV) and reaches our planet. In this regard, the studied ceramics can be promising as photocatalysts or light-absorbing elements of solar cells.

The results of studies of the electrical properties of the sample at room temperature are shown in Fig. 7. As can be seen from Fig. 6 a – c, three processes were observed in this sample. The low-frequency (LF) process manifested itself at frequencies below 300 Hz and was only partially present in the observation area. This is probably an ionic process. The mid-frequency (MF) process was observed in the frequency range from 300 Hz to 10 kHz. A high frequency (HF) process was observed from 100 kHz to 10 MHz. At low frequencies (≤10 kHz), a significant increase in the permittivity ε and a maximum dielectric loss (tan δ) were observed, which can be explained by the participation of adsorbed water in the polarization process, ionic polarization. The permittivity of the sample at room temperature and a frequency of 10^7 Hz reached high values of ≤147, while the dielectric loss tangent did not exceed 0.12. High dielectric losses may be due to the small grain size of ceramics, as well as the presence of adsorbed water, which can affect polarization processes at low temperatures (≤400°C). However, water can be present in various forms. In mesoporous samples, some of the water may be in a "liquid-like" state. At its core, this liquid is an electrolyte, which leads, firstly, to a giant dielectric constant, and secondly, to a rapid decrease in the dielectric constant with increasing frequency. The SP process is probably also associated with molecular water present in micropores. The RF process has a significant dielectric constant (about 150). Possibly, this process can also involve water, which is in the form of OH-groups on the surface of micropores or in the volume. In view of the foregoing, in order to understand the reasons for the giant values of the permittivity of ceramics, it is necessary to study the impedance during heating.

The modeling of the impedance hodograph has been carried out. Investigated serial and parallel equivalent circuits. As the assessment of modeling accuracy by the Pearson criterion showed, the serial ES showed low accuracy ($\chi^2 = 0.016$) compared to the parallel one. The parallel circuit for the frequency range 600 – 10^7 Hz turned out to be 7 times more accurate ($\chi^2 = 0.0022$). The high-precision sample equivalent circuit at 25°C includes the following parameters: $R_1 = 5636$ Om, $T_{CPE1} = 3\times10^{-10}$; $P_{CPE1} = 0.920$; $R_2 = 3838$ Om; $T_{CPE2} = 7.9\times10^{-8}$; $P_{CPE2} = 0.560$; W is the Warburg impedance, which manifests itself in the frequency range less than 300 Hz. Linear approximation by 4 points showed that the tangent of the slope angle is 0.48, which corresponds to the parameter $P \approx 0.5$. The second parameter of the Warburg impedance could not be determined due to the small number of points. Based on the simulation, we came to the conclusion that two fairly fast processes are observed. The second is probably due to ionics. The third, slowest process is probably due to water adsorbed in the pores.

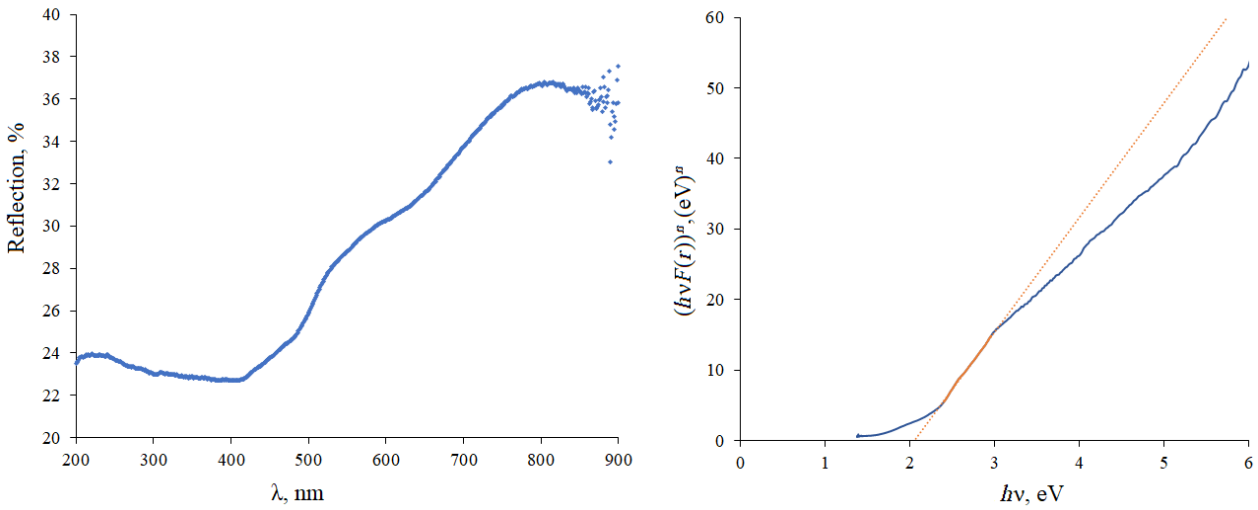

Fig. 6. (Color online) Diffuse reflection spectrum (a) and Tauc curve (b) for the $Pb_{1/3}Na_{1/3}K_{1/3}Ta_{2/3}Fe_{1/3}O_{3-\delta}$ sample.

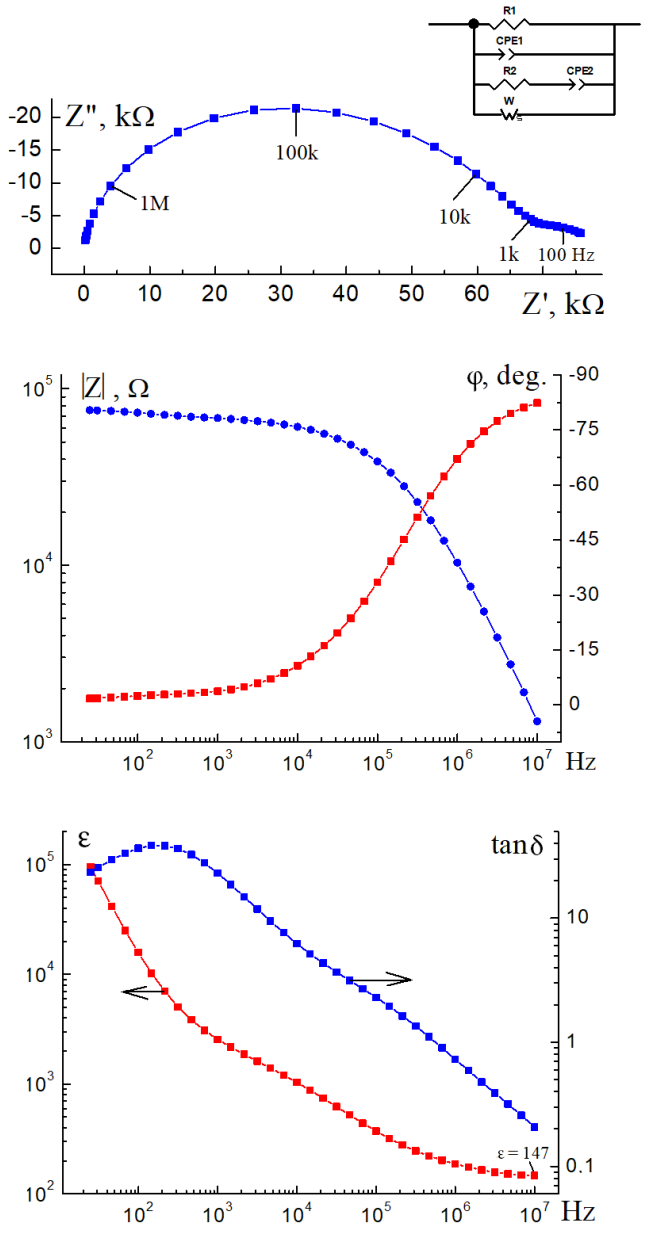

Fig. 7. (Color online) Hodograph of impedance; frequency dependences of the impedance modulus and phase angle, real part of the complex permittivity and dielectric loss tangent of the $Pb_{1/3}Na_{1/3}K_{1/3}Ta_{2/3}Fe_{1/3}O_{3-\delta}$ sample at 25°C.

4. Conclusions

For the first time, a phase-clean lead-containing complex oxide $Pb_{1/3}Na_{1/3}K_{1/3}Ta_{2/3}Fe_{1/3}O_{3-\delta}$ with a cubic perovskite structure (sp. gr. *Pm*-3*m*, $a = 3.9767(3)$ Å) was synthesized. The microstructure of the sample was formed by randomly oriented cubic crystallites. The band gap (≈2.05 eV) of the composite oxide was calculated. The permittivity of the sample at room temperature and a frequency of 10^7 Hz reached high values of ≈147, while the dielectric loss tangent did not exceed 0.12. The sample at room temperature exhibited three polarization processes in different frequency ranges: at a frequency of less than 300 Hz, in the frequency range from 300 Hz to 10 kHz, and from 100 kHz to 10 MHz.

References

1. S. Kawashima, M. Nishida, I. Ueda, H. Ouchi. J. Am. Ceram. Soc. 66 (6), 421 (1983). Crossref
2. A. Dutta, T. P. Sinha. Materials Research Bulletin, 46 (4), 518 (2011). Crossref
3. H. Tamura, T. Konoike, Y. Sakabe, K. Wakino. Communications of the American Ceramic Society. 67 (4), c59 (1984). Crossref
4. O. I. Prokopalo, I. P. Raevsky. Electrophysical properties of perovskite family oxides. Rostov University (1985) 104 p.
5. R. I. Scott, M. Thomas, C. Hampson. J. Eur. Ceram. Soc. 23, 2467 (2003). Crossref
6. S. B. Desu, H. M. O'bryan. J. Am. Ceram. Soc. 68 (10), 546 (1985). Crossref
7. A. S. Bhalla, R. Guo, R. Roy. Materials Research Innovations, 4 (1), 3 (2000). Crossref
8. P. K. Davies, T. Jianzhu. J. Am. Ceram. Soc. 80 (7), 1727 (1997). Crossref
9. F. Galasso, J. Pinto. Nature. 207 (4992), 70 (1965). Crossref
10. R. Zurmühlen, E. Colla, D. Dube, J. Petzelt, I. Reaney, A. Bell, N. Setter. Journal of Applied Physics. 76 (10), 5864 (1994). Crossref
11. F. Galasso, J. Pyle. Inorg. Chem. 2 (3), 482 (1963). Crossref
12. F. Galasso, J. Pyle. J. Phys. Chem. 67, 1561 (1963). Crossref
13. A. J. Jacobson, B. M. Collins, B. E. F. Fender. Inorg. Chem. 32 (4), 1083 (1976). Crossref
14. I.-T. Kim, T.-S. Oh, Y.-H. Kim. J Mater Sci Lett. 12, 182 (1993). Crossref
15. B.-K. Kim, H.-O. Hamaguchi, I.-T. Kim. J. Am. Ceram. Soc. 78, 3117 (1995). Crossref
16. R. Zurmühlen, J. Petzelt, S. Kamba, G. Kozlov, A. Volkov, B. Gorshunov, D. Dube, A. Tagantsev, N. Setter. Journal of Applied Physics. 77 (10), 5351 (1995). Crossref
17. T. Mitsuhiro, K. Kageyama. J. Am. Chem. Soc. 72 (10), 1955 (1989). Crossref
18. A. Dutta, T. Sinha. Physical Review B. 76 (15), 155113 (2007). Crossref
19. F. Galasso, L. Katz, R. Ward. J. Am. Chem. Soc. 81 (4), 820 (1959). Crossref
20. F. Galasso. The Journal of Chemical Physics. 44 (7), 2703 (1966). Crossref
21. W.-H. Jung, J.-H. Lee, J.-H. Sohn, H.-D. Nam, S.-H. Cho. Materials Letters. 56 (3), 334 (2002). Crossref
22. G. Li, S. Liu, F. Liao, S. Tian, X. Jing, J. Lin, Y. Uesu, K. Kohn, K. Saitoh, M. Terauchi, N. Di, Z. Cheng. J. Sol. St. Chem. 177 (4-5), 1695 (2004). Crossref
23. Z. Wang, X. M. Chen, L. Ni, Y. Y. Liu, X. Q. Liu. Applied Physics Letters. 90 (10), 102905 (2007). Crossref
24. S. P. Kubrin, S. I. Raevskaya, S. A. Kuropatkina, D. A. Sarychev, I. P. Raevski. Ferroelectrics. 340 (1), 155 (2006). Crossref
25. I. P. Raevski, S. A. Prosandeev, S. A. Bogatina, M. A. Malitskaya, L. Jastrabik. Integrated Ferroelectrics. 55 (1), 757 (2003). Crossref
26. L. G. Akselrud, Yu. N. Grin, P. Yu. Zavalij, et al. CSD-universal program package for single crystal or powder structure data treatment. Thes. Rep. XII Eur. Crystallogr. Meet. (1989) p. 155.

27. R. D. Shannon. Acta Crystallogr. A. 32, 751 (1976). Crossref
28. M. J. Whitaker, J. F. Marco, F. J. Berry, C. Raith, E. Blackburn, C. Greaves. J. Solid St. Chem. 198, 316 (2013). Crossref
29. F. A. Jusoh, K. B. Tan, Z. Zainal, S. K. Chen, C. C. Khaw, O. J. Lee. J. Asian Ceram. Soc. 8, 957 (2020). Crossref
30. N. A. Zhuk, V. P. Lutoev, V. A. Belyy, B. A. Makeev, D. S. Beznosikov, S. V. Nekipelov, M. V. Yermolina. Phys. B: Condensed Matter. 552, 142 (2019). Crossref
31. S. A. Ivanov, P. Nordblad, R. Tellgren, T. Ericsson, H. Rundlof. Solid State Sciences. 9 (5), 440 (2007). Crossref
32. T. Yamashita, P. Hayes. Appl. Surface Sci. 254 (8), 2441 (2008). Crossref
33. J. F. Moulder. Handbook of X-ray Photoelectron Spectroscopy: A Reference Book of Standard Spectra for Identification and Interpretation of XPS Data. Physical Electronics Division, Perkin-Elmer Corporation (1992) 261 p.
34. Subhashini, H. D. Shashikala, N. K. Udayashankar. Ceram. Intern. 46 (4), 5213 (2020). Crossref